Renewable Energy from Livestock Waste Valorization: Amyloid-Based Feather Keratin Fuel Cells

Ali Miserez (ali.miserez@ntu.edu.sg)
Nanyang Technological University https://orcid.org/0000-0003-0864-8170
Wei Long Soon
Nanyang Technological University
Mohammad Peydayesh
ETH Zürich https://orcid.org/0000-0002-6265-3811
Tym de Wild
Electrochemistry Laboratory, Paul Scherrer Institut https://orcid.org/0000-0002-6412-6548
Felix Donat
Department of Mechanical and Process Engineering, ETH Zürich
Rinku Saran
Nanyang Technological University
Christoph Müller
Laboratory of Energy Science and Engineering, ETH Zürich
Lorenz Gubler
Electrochemistry Laboratory, Paul Scherrer Institut
Raffaele Mezzenga
ETH Zurich https://orcid.org/0000-0002-5739-2610

Physical Sciences - Article

Keywords:

Posted Date: June 12th, 2023

DOI: https://doi.org/10.21203/rs.3.rs-2816640/v1

Abstract

Increasing carbon emissions have accelerated climate change, resulting in devastating effects that have become tangible on an everyday basis[1]. This is mirrored by a projected increase in global energy demand by *ca.* 50% in a single generation timespan[2,3], urging a shift from fossil-fuel derived materials toward greener materials and more sustainable manufacturing processes[4]. Bio-based industrial byproducts, such as food industry side-streams[5], are attractive alternatives with a strong potential for valorization owing to their large volume, low cost, renewability, biodegradability, and intrinsic material properties[6]. Here we demonstrate the reutilization of industrial chicken feathers waste into proton conductive membranes for fuel cells[7], protonic transistors[8], and water-splitting devices[9]. Keratin was isolated from chicken feathers via a fast and economical process, converted into amyloid fibrils upon heat treatment, and further processed into membranes with imparted proton conductivity through a simple oxidative method[10]. The functionality of the membranes is demonstrated by assembling them into a hydrogen fuel cell capable of powering several types of devices using hydrogen and air as fuel. Additionally, these membranes could be used to generate hydrogen by water splitting, and in protonic field-effect transistors as a thin-film modulating protonic conductivity via the electrostatic gating effect. We believe that by converting industrial waste into renewable energy materials at low cost and high scalability, our green manufacturing process can contribute to a fully circular economy with neutral carbon footprint.

Full Text

Global energy demand has been on the continuous rise and is anticipated to further increase by an astonishing 47% in the near future[2]. Current primary energy sources, which are still derived from non-renewable fossil fuels, are unsustainable and detrimental to the environment due to the large emissions of greenhouse gases (GHG) into the atmosphere. Hence, to curb global warming, there is an urgent need for new technologies based on renewable and sustainable energy generation sources.

Fuel cells are considered a promising sustainable technology for energy conversion to generate electricity without CO_2 emissions using electrochemical reactions[11]. Among the various types of fuel cells, hydrogen fuel cells are particularly attractive from a decarbonization point-of-view, with efforts focusing on the production of green hydrogen as the next renewable fuel[12]. The heart of a fuel cell lies in the membrane electrode assembly (MEA), which consists of a proton exchange membrane (PEM) that selectively allows only the passage of protons between the electrodes. Perfluorosulfonic acid (PFSA) membranes such as NafionÔ and AquivionÒ remain the benchmark state-of-the-art PEMs used in fuel cells due to their high proton conductivity, chemical inertness, and mechanical stability. However, the production of Nafion is very expensive due to the use of fluorinated chemicals[13] and pose serious environmental concerns relating to poor biodegradability and environmental toxicity of perfluorinated materials[14]. Moreover, the functionalization of polymers through sulfonation usually involve highly corrosive reagents, reducing their environmental friendliness,[15-17] boosting the search for greener and more economical materials for large-scale applications.

Inspired by the ubiquity of proton conduction in the living world[18,19] as well as their intrinsic biodegradability, studies have explored biopolymers (proteins and polysaccharides) as potential proton conductive materials[20,21]. The proton conductivity of naturally occurring proteins is generally too low to be useful in practical applications but has been improved with functional group modifications[8,22]. Alternatively, high proton conductivity can be achieved in biopolymers through *de novo* design of peptides utilizing nanostructure-aided conductivity[23] or metal oxide-peptide composites [24], but these approaches still face challenges regarding cost and scalability.

Chicken feathers are produced at a staggering rate of 40 million tons annually as a byproduct from the poultry industry[5], but have been underutilized due to their unsuitable nutritional profile. Furthermore, they face disposal challenges due to the generation of toxic sulfur dioxide from incineration. Efforts to valorize chicken feathers include their use as hydrogels[25,26], biosorbents for heavy metals[27,28], functional films[29] and fibers[30]. These studies point out that feather keratin may be re-configured into highly functional materials, notably exploiting the structural properties and high cysteine (Cys) content of keratin proteins. However, no attempts have been made to date to revalue keratin into renewable energy devices. In this work, we chose chicken feathers as a starting material for fabricating proton conductive biomaterials. Keratin proteins were extracted from industrial chicken feathers using an environmentally friendly and scalable process and converted into amyloid fibrils that were subsequently processed into free-standing amyloid fibril membranes. Proton conductive properties were imparted through a post-oxidative treatment which converted Cys thiols into sulfonic acid groups, using a benign environmental process with harmless and inexpensive chemical compounds. The performance of the membrane was demonstrated in a fuel cell device capable to transform by electrochemical reaction H_2 and O_2 (the latter directly from air) into electrical power and mechanical work (with H_2O as sole byproduct). To demonstrate the general potential of this approach, we highlight two additional applications of these materials, as protonic field-effect transistors, as well as in the generation of H_2 via water splitting.

Protein extraction and isolation

An overview of the production of feather keratin proton conductive membranes is depicted in Fig. 1. Keratin was extracted and isolated from chicken feathers and heat treated to produce keratin amyloid fibrils (Fig. 1a), after which they were mixed with a crosslinker and dopant and cast onto a substrate to produce a free-standing membrane. The membrane was then heat cured followed by an oxidative treatment to produce a modified membrane with imparted proton conductive properties (Fig. 1b), which was then assembled into a fuel cell (Fig. 1c) or other devices utilizing proton conductivity.

Among protein-containing industrial waste byproducts, chicken feathers have the highest protein content (*ca.* 90%) and are most abundant in Cys amino acid (*ca.* 8%, Fig. 2a)[5]. However, the extraction and isolation procedure of feather keratin on a large scale has faced challenges, notably the use of harsh toxic solvents (e.g. sodium sulfide) and reducing agents such as b-mercaptoethanol and dithiothreitol, or long isolation dialysis treatments[31]. Here, we extracted feather keratin using a basic solvent consisting of

urea and thioglycolate. Urea acted as a chaotropic solvent disrupting the hydrogen bonds within the compact structure of feathers, while thioglycolate served as a reducing agent to reduce intra- and intermolecular disulfide bonds, resulting in the separation of protein inter-chains and eventually dissolution. The supernatant was then precipitated and washed to obtain a crude keratin isolate. We re-extracted this isolate in ammoniacal solution and precipitated it to obtain a pure keratin isolate, which displayed only a single protein band around 10 kDa as analyzed by electrophoresis (Fig. 2b), demonstrating minimal protein degradation during the entire process. An amino acid analysis of the obtained keratin isolate revealed 7 mol.% of Cys (Supplementary Fig. S1), in agreement with the expected 8 mol.% from earlier reports[32]. Our process produced a feather keratin isolate almost fully soluble in dilute acid, in contrast to keratin isolates obtained from other extraction procedures, which require concentrated acids[33]. Furthermore, the process does not require dialysis, enabling scalability and fast production rates.

Protein fibrillization

Within the family of keratin proteins, hair and wool keratins belong to a-keratins composed of a-helix intermediate filaments, while keratin from feathers, claws, and beaks belong to b-keratins dominated by b-sheet secondary structures[34,35]. While early x-ray diffraction (XRD) studies on feather barbs suggested the presence of amyloid-like fibrils[36], the self-assembly of regenerated feather keratin into amyloid fibrils has not yet been reported to date. Sequence analysis of feather keratin from the UniProt database (P02450) using a variety of protein structure prediction algorithms (Supplementary Fig. S2) indicated that feather keratin could be assembled into amyloid fibrils. The structure of feather keratin has been reported to consist of a central region with predominantly hydrophobic residues adopting a b-sheet conformation[32], with Cys residues primarily located at the N- and C-termini[37]. The highest propensity for b-sheet aggregation was predicted to occur between residues Val[32]–Leu[43], which lie within this central region and have also been identified as a hotspot for amyloidogenic aggregation. Thus, we postulated that feather keratin could be self-assembled into amyloid fibrils, which was verified by the facile self-assembly of keratin monomers into amyloid fibrils after heat treatment at 90°C under acidic conditions. Using thiazole orange as a molecular probe for amyloid fibrils[38], the fibrillization process proceeded relatively quickly and reached a plateau after only 2h, exhibiting a faster kinetic than that of animal-derived b-lactoglobulin[39] or plant-derived proteins[40] (Fig. 2c). Solutions of feather keratin amyloid fibrils also exhibited birefringence under cross-polarized light, corroborating the presence of amyloid fibrils (inset of Fig. 2c), which were found to be several micrometers in length after 5h as imaged by Atomic Force Microscopy (AFM) and Transmission Electron Microscopy (TEM) (Fig. 2d and 2i). The nanofibrils exhibited an average height of about 7 nm (Fig. 2e), a semiflexible behavior with comparable contour (Fig. 2f) and persistence (Fig. 2g) lengths in the range, and periodic pitches of 90 nm along the fibril axis (Fig. 2h), as expected for most amyloid fibrils.

Membrane fabrication

We then mixed feather keratin amyloid fibrils with glyoxal and mercaptosuccinic acid and cast the solution to obtain a clear free-standing flexible membrane (Supplementary Fig. S3a), followed by thermal curing (Supplementary Fig. S3b). As we hypothesized that proton conduction could be imparted into the membrane upon conversion of thiol groups into sulfonic acids, we immersed the membranes in peracetic acid to oxidize thiols and disulfide bonds to sulfonic acids (Supplementary Fig. S3c)[10,41]. The final membrane is denoted as Keratin-M.

Oxidation into sulfonic acid was corroborated by both Fourier Transform Infrared Spectroscopy (FTIR) and Raman Spectroscopy, with the appearance of the S=O peak at 1040 cm^{-1} [42] (Fig. 3a) in the FTIR spectrum, and the disappearance of the Raman shift peak at 2550 cm^{-1} assigned to the thiol[43] (Fig. 3b). This was further supported by XPS measurements, which showed the major peaks of $-SO_3^-$ $2p_{3/2}$ and $2p_{1/2}$ doublets at 168.2 and 169.6 eV, respectively, after deconvolution[44-47]. Peaks of sulfone and sulfate groups were also observed, possibly due to side reactions in the fabrication process (Fig. 3c). As the modification of thiols into sulfonic acids confers a negative charge, the difference in surface potential before and after modification was detected by Kelvin Probe Force Microscopy (KPFM). Before modification, the keratin casting solution deposited onto the Highly Oriented Pyrolytic Graphite (HOPG) substrate exhibited a relative positive potential, which likely arose from positively charged amino acids Arg and Lys. Upon oxidative treatment, the membrane exhibited a relative negative potential that may have resulted from the conversion of neutral thiols into negatively charged sulfonic acids (Fig. 3d and Supplementary Fig. S5).

Throughout the fabrication process, the membrane maintained its shape and mechanical integrity while still possessing birefringence arising from amyloid fibrils under cross-polarized light (Supplementary Fig. S3d), suggesting that the amyloid fibrils were preserved without significant alteration. The XRD pattern of the membranes displayed two dominant peaks at 9.3° and 19.6°, corresponding to *d*-spacings of 4.5 Å and 9.5 Å, respectively, that reflect the signature cross-b structure of amyloid fibrils[48,49] (Fig. 3e). A smooth surface was observed under SEM for keratin-M membranes (Supplementary Fig. S6), whereas at higher magnification a fibrillar network morphology was identified on the surface with pore sizes of 7–20 nm (Fig. 3f). In contrast, neat keratin membranes showed a denser morphology with lower porosity (Supplementary Fig. S7).

Membrane properties

The modification of neutral thiols into negatively charged sulfonic acids was also indicated by the increase in ion exchange capacity (IEC) from 0.18 meq g^{-1} to 0.84 meq g^{-1} after oxidative treatment, while a further increase to 1.56 meq g^{-1} was achieved with the addition of MSA due to the contribution of additional thiol groups (Table 1). The boost in IEC also resulted in a higher water uptake due to enhanced hydration and charge repulsion from the anionic sulfonic acid groups, which could possibly explain the larger pore size from keratin-M due to higher swelling compared to neat keratin membranes. Keratin-M membranes maintained good barrier properties despite the presence of nanopores, demonstrating almost

no permeability to dye molecules such as Rhodamine B (Supplementary Fig. S8). They also exhibited 3-fold less permeability to small molecules such as methanol compared to Nafion (Supplementary Fig. S9), demonstrating their potential in direct methanol fuel cells in which Nafion performs less efficiently due to its high methanol permeability[50]. The membranes were mechanically robust and could be readily manipulated without damaging them. Their thermo-mechanical characterization is reported in the supplementary information (Young's Modulus and tensile strength in Supplementary Table S1 and Fig. S10; thermal behavior and glass transition in Fig. S11). Supercritical CO_2-dried keratin membranes measured with TGA displayed a 10% decrease in weight until 100°C attributed to the evaporation of water, followed by thermal degradation and deamidation with drastic weight loss (~ 60%) between 300°C to 400°C[51] (Supplementary Fig. S12).

Table 1. Feather keratin membrane properties before and after treatment

Membrane	IEC (meq g^{-1})	Water Uptake (%)
Pre-treated	0.18 ± 0.03	55.3 ± 6.7
Neat keratin	0.84 ± 0.05	131.3 ± 17
Keratin-M	1.56 ± 0.03	215.9 ± 31
Nafion 117	1.10 ± 0.02	17.0 ± 1.2

The main parameter in a fuel cell is the proton conductivity (s), which is essential for any polymer electrolyte membrane. After the successful conversion of thiols into sulfonic acids, feather keratin membranes exhibited an enhanced proton conductivity that increased with the MSA content from 0.02 mS cm^{-1} to 6.3 mS cm^{-1} in water (Fig. 4a). The appearance of the semi-circle in the Nyquist plot of neat membranes indicate a more capacitive behavior (Fig. 4b), as also evidenced in the large phase angle from the Bode plot (Supplementary Fig. S13a). This characteristic shifted towards a membrane with a resistor-type behavior for keratin-M membranes, as seen from an almost absent semi-circle in the Nyquist plot (Fig. 4c) and a phase angle approaching 0° at high frequencies in the Bode plot (Supplementary Fig. S13b). Comparing across biomaterials reported to date, the proton conductivity of keratin-M is the highest among all biopolymers, with the exception of specifically engineered peptides (Supplementary Table S2 and S3). But in contrast to the latter, feather keratin membranes are processed from low-value waste materials with a strong potential for scaling-up. Remarkably, because this comes from a waste stream intended for incineration (and CO_2 emissions), this process takes place with an overall negative carbon footprint, adding value to both sustainability and environmental friendliness. Furthermore, the proton conductivity of the membranes could still be further improved by doping with acid electrolytes, notably with sulfuric acid which provided the most significant increment to 22.8 mS cm^{-1}, and which may find applications in vanadium redox flow batteries.

Fuel cell performance

Having demonstrated a suitable proton conductivity for the ensued amyloid keratin membranes, we then tested their *in-situ* performance as a polymer electrolyte membrane in a hydrogen fuel cell (Supplementary Fig. S14). The open circuit voltage (OCV) of a fuel cell has been reported to provide a useful indication of the integrity and degradative behavior of the membrane such as thinning and pinhole formation[52]. The cell assembled with keratin-M membrane displayed an OCV between 0.95 – 1 V – comparable to Nafion – and polarization curves were obtained at increasing temperature. With air at the cathode, the cell generated an increased power density with temperature, reaching up to 20 mW cm^{-2} at 65°C (Fig. 4d). Similarly, the peak power of 25 mW cm^{-2} was generated with pure oxygen at 55°C, after which it decreased to 21 mW cm^{-2} at 65°C (Fig. 4e). This could be due to an increase in reactive oxygen species generated with increased oxygen concentration, leading to the formation of free radicals such as OH×, H×, and HOO× that have been reported to initiate membrane degradation[53,54]. Further increase in temperature to 80°C resulted in a drop in OCV to 0.85 – 0.9 V along with a decreased power density lower than that at 65°C. To ensure a high OCV and optimal performance, a membrane of low hydrogen permeability is desired. Utilizing staircase voltammetry with N_2 at the cathode (Supplementary Fig. S16), the hydrogen permeability of the keratin membrane was assessed and calculated using the intercept, yielding 3.8 ± 0.3 ´ 10^{-10} mol cm^{-2} s^{-1}, (compare to Nafion - 3.8 ´ 10^{-9} mol cm^{-2} s^{-1})[55] while the electrical resistance obtained from the slope was approximately 3200 ± 140 Ohm cm^2 (Supplementary Fig. S17)[56,57].

To demonstrate the applicability of the keratin-M membrane in hydrogen fuel cells, we assembled the membrane into a commercial test fuel cell setup. With hydrogen and air as the respective fuels at the anode and cathode, the cell was able to generate power to turn on both red and white LED lamps (Supplementary Fig. S18). In addition, the cell was responsive to the presence of fuel, turning the LED lamp on and off with the introduction and absence of hydrogen (Supplementary Movie S1). Most importantly, the fuel cell could perform mechanical work, *e.g.* drive a fan setup driven by a motor (Supplementary Movie S2) as well as a fuel cell toy car ((Supplementary Movie S4 and Fig. 4f). Furthermore, the keratin-M PEM membranes could be further used as an electrolyzer for the production of hydrogen and oxygen from water when applying an electric bias, as observed by the formation of bubbles at the respective outlets (Supplementary Movie S4 & Supplementary Fig. S19).

Transistor performance

Finally, we demonstrate the application of keratin-M as a solid-state film for the fabrication of protonic field-effect transistors (H^+-FETs). Devices were fabricated by casting keratin-M film between two gold/palladium hydride (PdH_x) electrodes pre-deposited using e-beam evaporation process on a 50 nm hafnium oxide (HfO_2) gate dielectric layer (Fig. 4g). The conductivity of the keratin-M film was observed to be dependent on relative humidity (RH), displaying a surge in current when the RH increased from 50% to 90% (Fig. 4h and Supplementary Fig. S20), as a result of the increase in proton conductivity with increased hydration, which is commonly observed in most proton conductive materials[20,22,58]. The transfer characteristics of the FET device (Fig. 4i) measured for negative and positive gate voltages (V_{GS})

at a source to drain voltage (V_{SD}) of 0.5 V exhibited a ON-to-OFF ratio of ~ 1.4 with a low leakage current (Supplementary Fig. 21). The output characteristics of the device displayed a similar trend whereby the channel conductivity increased upon application of negative V_{GS} (Supplementary Fig. 23 and 24). Biasing the device with negative V_{GS} induced positive charges into the channel proportional to V_{GS} as the keratin-M and Si gate form a capacitor with HfO_2 as the dielectric. This resulted in an increased positive charge carrier concentration and thereby channel conductivity. The electrostatic gating effect highlights the potential use of keratin-M in H^+-FETs.

Conclusions

We have demonstrated the fabrication of proton conductive membranes isolated from chicken feathers keratin through a green and low-cost process with high scalability. Amyloid-based keratin membranes were successfully used in a hydrogen fuel cell to power several devices with only hydrogen and air as the fuel, and also demonstrated pronounced electrostatic gating effect in a transistor and hydrogen generation in an electrolyzer. While the ensued proton conductive membranes do not yet fully match the performance (particularly at high temperature) of commercial benchmarks such as NafionÔ and AquivionÒ, the membranes pose a radically different environmental and sustainability footprint and at a potentially much lower cost: our current estimates on the total production from raw material to membrane give *ca*. USD 850/m^2. This value is at least half that of NafionÔ (USD 1500 – 3000/m^2) and is anticipated to be much lower when scaled up and optimized, hence highlighting another long sought-after feature of these original materials. Our study unambiguously demonstrates that livestock industrial waste can be reprocessed into valuable materials for renewable energy devices using a fully sustainable process, and brings us one step closer towards a circular economy concept based on zero -or even negative- carbon emissions.

Materials and Methods

Full details on Materials and Methods are provided in the Supporting Sections A-D. Hereby a summary of the main methods used is provided.

Protein extraction and isolation to membrane fabrication

Protein extraction and isolation from chicken feathers obtained from a local farm are detailed in Supplementary Section AI. Feather keratin amyloid fibrils were prepared by heating keratin isolates (Supplementary Section AII) and fabricated into membranes as described in Supplementary Section AIII. Protein and membrane characterization are provided in Supplementary Section B and C, respectively. Electrochemical measurements of membranes are described in Supplementary Section D.

Fuel cell measurements

For the in-situ fuel cell measurements, membranes were placed inside a 1 cm^2 cell between two platinum-coated commercial GDE's (JM ELE0244, Johnson Matthey, United Kingdom) with a nominal loading of 0.4 mg Pt/cm^2. Fuel cell tests were performed using a custom fuel cell test bench with a constant flow rate of 0.4 ln/min for all gasses. Polarization curves were recorded at 100% RH and a pressure of 1.5 bar. Hydrogen crossover currents were measured using staircase voltammetry at 100% RH and a pressure of 1 bar. Additional details are provided in Supplementary Section IV. To demonstrate powering of the devices, membranes were placed between two platinum-coated carbon paper electrodes of 0.5 mg/cm^2 (Fuel Cell Store, USA) to form the membrane electrode assembly in the Flex-Stak Electrochemical cell (Fuel Cell Store, USA). Pure H_2 and Air were supplied at the anode and cathode, respectively. Metal tabs were connected to a mini DC/DC (LiPower, Sparkfun) converter with an output of 3.3 V.

Transistor fabrication

Field-effect transistor devices (channel length of 100 mm and width of 1 mm) were fabricated by depositing gold/palladium metal electrodes using electron-beam evaporation on top of hafnium oxide (50 nm) coated silicon substrate. Palladium electrodes were exposed to pure hydrogen gas for 5 mins in a closed chamber for their transformation to PdH_x. 0.5 mL of amyloid fibril mixed with glyoxal and MSA were deposited onto the device and air-dried. The substrate was then cured at 150°C for 50 min and immersed in peracetic acid solution at 37°C for 5 h. The device was then immersed in 0.5 M sulfuric acid for 1 h and then rinsed thoroughly with water.

H^+-FET Characterization

Output and transfer characteristic of the transistor devices were recorded using the Keysight B2901A precision source measure unit. Relative humidity level was kept at 95% in a custom-built dry box chamber using a humidifier (BioAire Lifestyle).

Declarations

Acknowledgements

This research was supported by the strategic initiative on biomimetic and sustainable materials (IBSM), Nanyang Technological University (NTU), Singapore. W.L.S thanks NTU Singapore for the Nanyang President Graduate Scholarship (NPGS). The authors acknowledge the support of Dr. Anne Greet Bittermann and Stephan Handschin of ScopeM/ETH Zurich. The authors thank Prof. Nripan Matthews and Dr. Timothy Ng for the use of e-beam deposition system and Prof. Cesare Soci group for the use of source measurement unit for characterization of FETs.

Conflict of Interest

R.M., W.L.S., and A.M. are the inventors of a patent application jointly filed by NTU and ETHZ.

Author Contributions

W.L.S., R.M and A.M. designed the study. W.L.S. carried out the experiments from protein extraction and isolation to membrane fabrication and characterization. T.D.W and L.G. carried out the in-situ fuel cell measurements. F.D. carried out the TGA and XRD measurements. W.L.S. and F.D. carried out the commercial fuel cell device demonstration. R.S. carried out the transistor performance measurements. A.M., R.M., and M.P. supervised the study. W.L.S., A.M., and R.M. wrote the manuscript. All the authors edited and approved the final manuscript.

Data Availability

The authors declare that the data supporting the findings of this study are available within the paper and its Supplementary Information files. Should any raw data files be needed in another format they are available from the corresponding author upon reasonable request.

References

1. Rockström, J. *et al.* A safe operating space for humanity. *Nature* **461**, 472-475 (2009). https://doi.org:10.1038/461472a
2. Meghan, G. & Weber, M. Global energy demand to grow 47% by 2050, with oil still top source: US EIA. (2021). <https://www.spglobal.com/commodityinsights/en/market-insights/latest-news/oil/100621-global-energy-demand-to-grow-47-by-2050-with-oil-still-top-source-us-eia>.
3. IEA. Global electricity demand is growing faster than renewables, driving strong increase in generation from fossil fuels. (2021). <https://www.iea.org/news/global-electricity-demand-is-growing-faster-than-renewables-driving-strong-increase-in-generation-from-fossil-fuels>.
4. Forum, W. E. Here's why green manufacturing is crucial for a low-carbon future. (2019). <https://www.weforum.org/agenda/2019/01/here-s-why-green-manufacturing-is-crucial-for-a-low-carbon-future/>.
5. Peydayesh, M., Bagnani, M., Soon, W. L. & Mezzenga, R. Turning Food Protein Waste into Sustainable Technologies. *Chemical Reviews* (2022). https://doi.org:10.1021/acs.chemrev.2c00236
6. Jana, S. *et al.* Waste-derived biomaterials as building blocks in the biomedical field. *Journal of Materials Chemistry B* **10**, 489-505 (2022). https://doi.org:10.1039/D1TB02125G
7. Edwards, P. P., Kuznetsov, V. L., David, W. I. F. & Brandon, N. P. Hydrogen and fuel cells: Towards a sustainable energy future. *Energy Policy* **36**, 4356-4362 (2008). https://doi.org:https://doi.org/10.1016/j.enpol.2008.09.036
8. Zhong, C. *et al.* A polysaccharide bioprotonic field-effect transistor. *Nature Communications* **2**, 476 (2011). https://doi.org:10.1038/ncomms1489
9. Shiva Kumar, S. & Himabindu, V. Hydrogen production by PEM water electrolysis – A review. *Materials Science for Energy Technologies* **2**, 442-454 (2019). https://doi.org:https://doi.org/10.1016/j.mset.2019.03.002

10. Du, P., Liu, W., Cao, H., Zhao, H. & Huang, C.-H. Oxidation of amino acids by peracetic acid: Reaction kinetics, pathways and theoretical calculations. *Water Research X* **1**, 100002 (2018). https://doi.org:https://doi.org/10.1016/j.wroa.2018.09.002
11. Fan, L., Tu, Z. & Chan, S. H. Recent development of hydrogen and fuel cell technologies: A review. *Energy Reports* **7**, 8421-8446 (2021). https://doi.org:https://doi.org/10.1016/j.egyr.2021.08.003
12. van Renssen, S. The hydrogen solution? *Nature Climate Change* **10**, 799-801 (2020). https://doi.org:10.1038/s41558-020-0891-0
13. Stropnik, R., Lotrič, A., Bernad Montenegro, A., Sekavčnik, M. & Mori, M. Critical materials in PEMFC systems and a LCA analysis for the potential reduction of environmental impacts with EoL strategies. *Energy Science & Engineering* **7**, 2519-2539 (2019). https://doi.org:https://doi.org/10.1002/ese3.441
14. Conley, J. M. *et al.* Developmental toxicity of Nafion byproduct 2 (NBP2) in the Sprague-Dawley rat with comparisons to hexafluoropropylene oxide-dimer acid (HFPO-DA or GenX) and perfluorooctane sulfonate (PFOS). *Environment International* **160**, 107056 (2022). https://doi.org:https://doi.org/10.1016/j.envint.2021.107056
15. Erce, Ş. *et al.* Effects of sulfonated polyether-etherketone (SPEEK) and composite membranes on the proton exchange membrane fuel cell (PEMFC) performance. *International Journal of Hydrogen Energy* **34**, 4645-4652 (2009). https://doi.org:https://doi.org/10.1016/j.ijhydene.2008.08.066
16. Khomein, P., Ketelaars, W., Lap, T. & Liu, G. Sulfonated aromatic polymer as a future proton exchange membrane: A review of sulfonation and crosslinking methods. *Renewable and Sustainable Energy Reviews* **137**, 110471 (2021). https://doi.org:https://doi.org/10.1016/j.rser.2020.110471
17. Park, C. H., Lee, C. H., Guiver, M. D. & Lee, Y. M. Sulfonated hydrocarbon membranes for medium-temperature and low-humidity proton exchange membrane fuel cells (PEMFCs). *Progress in Polymer Science* **36**, 1443-1498 (2011). https://doi.org:https://doi.org/10.1016/j.progpolymsci.2011.06.001
18. Josberger, E. E. *et al.* Proton conductivity in ampullae of Lorenzini jelly. *Science Advances* **2**, e1600112 (2016). https://doi.org:doi:10.1126/sciadv.1600112
19. Ordinario, D. D. *et al.* Bulk protonic conductivity in a cephalopod structural protein. *Nature Chemistry* **6**, 596-602 (2014). https://doi.org:10.1038/nchem.1960
20. Guccini, V. *et al.* Highly proton conductive membranes based on carboxylated cellulose nanofibres and their performance in proton exchange membrane fuel cells. *Journal of Materials Chemistry A* **7**, 25032-25039 (2019). https://doi.org:10.1039/C9TA04898G
21. Baumgartner, M. *et al.* Resilient yet entirely degradable gelatin-based biogels for soft robots and electronics. *Nature Materials* **19**, 1102-1109 (2020). https://doi.org:10.1038/s41563-020-0699-3
22. Nandi, R., Agam, Y. & Amdursky, N. A Protein-Based Free-Standing Proton-Conducting Transparent Elastomer for Large-Scale Sensing Applications. *Advanced Materials* **33**, 2101208 (2021). https://doi.org:https://doi.org/10.1002/adma.202101208
23. Ma, C. *et al.* De novo rational design of a freestanding, supercharged polypeptide, proton-conducting membrane. *Science Advances* **6**, eabc0810 (2020). https://doi.org:doi:10.1126/sciadv.abc0810

24. Lee, J. *et al.* Proton Conduction in a Tyrosine-Rich Peptide/Manganese Oxide Hybrid Nanofilm. *Advanced Functional Materials* **27**, 1702185 (2017). https://doi.org:https://doi.org/10.1002/adfm.201702185
25. Esparza, Y., Bandara, N., Ullah, A. & Wu, J. Hydrogels from feather keratin show higher viscoelastic properties and cell proliferation than those from hair and wool keratins. *Materials Science and Engineering: C* **90**, 446-453 (2018). https://doi.org:https://doi.org/10.1016/j.msec.2018.04.067
26. Wang, J. *et al.* Feather keratin hydrogel for wound repair: Preparation, healing effect and biocompatibility evaluation. *Colloids and Surfaces B: Biointerfaces* **149**, 341-350 (2017). https://doi.org:https://doi.org/10.1016/j.colsurfb.2016.10.038
27. Khosa, M. A., Wu, J. & Ullah, A. Chemical modification, characterization, and application of chicken feathers as novel biosorbents. *RSC Advances* **3**, 20800-20810 (2013). https://doi.org:10.1039/C3RA43787F
28. Sun, P., Liu, Z.-T. & Liu, Z.-W. Chemically Modified Chicken Feather as Sorbent for Removing Toxic Chromium(VI) Ions. *Industrial & Engineering Chemistry Research* **48**, 6882-6889 (2009). https://doi.org:10.1021/ie900106h
29. Tsuda, Y. & Nomura, Y. Properties of alkaline-hydrolyzed waterfowl feather keratin. *Animal Science Journal* **85**, 180-185 (2014). https://doi.org:https://doi.org/10.1111/asj.12093
30. Ma, B., Qiao, X., Hou, X. & Yang, Y. Pure keratin membrane and fibers from chicken feather. *International Journal of Biological Macromolecules* **89**, 614-621 (2016). https://doi.org:https://doi.org/10.1016/j.ijbiomac.2016.04.039
31. Shavandi, A., Silva, T. H., Bekhit, A. A. & Bekhit, A. E.-D. A. Keratin: dissolution, extraction and biomedical application. *Biomaterials Science* **5**, 1699-1735 (2017). https://doi.org:10.1039/C7BM00411G
32. Arai, K. M., Takahashi, R., Yokote, Y. & Akahane, K. Amino-Acid Sequence of Feather Keratin from Fowl. *European Journal of Biochemistry* **132**, 501-507 (1983). https://doi.org:https://doi.org/10.1111/j.1432-1033.1983.tb07389.x
33. Aluigi, A. *et al.* Study on the structure and properties of wool keratin regenerated from formic acid. *International Journal of Biological Macromolecules* **41**, 266-273 (2007). https://doi.org:https://doi.org/10.1016/j.ijbiomac.2007.03.002
34. Fraser, R. D. B. & Parry, D. A. D. The role of β-sheets in the structure and assembly of keratins. *Biophys Rev* **1**, 27 (2009). https://doi.org:10.1007/s12551-008-0005-0
35. Meyers, M. A., Chen, P.-Y., Lin, A. Y.-M. & Seki, Y. Biological materials: Structure and mechanical properties. *Progress in Materials Science* **53**, 1-206 (2008). https://doi.org:https://doi.org/10.1016/j.pmatsci.2007.05.002
36. Filshie, B. K., Fraser, R. D., Macrae, T. P. & Rogers, G. E. Appendix-X-ray-diffraction and electron-microscope observations on soluble derivatives of feather keratin. *Biochem J* **92**, 18.12-19 (1964). https://doi.org:10.1042/bj0920018

37. Schrooyen, P. M. M., Dijkstra, P. J., Oberthür, R. C., Bantjes, A. & Feijen, J. Partially Carboxymethylated Feather Keratins. 1. Properties in Aqueous Systems. *Journal of Agricultural and Food Chemistry* **48**, 4326-4334 (2000). https://doi.org:10.1021/jf9913155
38. Gao, G.-Q. & Xu, A.-W. A new fluorescent probe for monitoring amyloid fibrillation with high sensitivity and reliability. *RSC Advances* **3**, 21092-21098 (2013). https://doi.org:10.1039/C3RA43259A
39. Shen, Y. *et al.* Amyloid fibril systems reduce, stabilize and deliver bioavailable nanosized iron. *Nature Nanotechnology* **12**, 642-647 (2017). https://doi.org:10.1038/nnano.2017.58
40. Soon, W. L., Peydayesh, M., Mezzenga, R. & Miserez, A. Plant-based amyloids from food waste for removal of heavy metals from contaminated water. *Chemical Engineering Journal* **445**, 136513 (2022). https://doi.org:https://doi.org/10.1016/j.cej.2022.136513
41. Li, J. *et al.* Foaming, emulsifying properties and surface hydrophobicity of soy proteins isolate as affected by peracetic acid oxidation. *International Journal of Food Properties* **22**, 689-703 (2019). https://doi.org:10.1080/10942912.2019.1602540
42. Kuzuhara, A. Analysis of structural changes in bleached keratin fibers (black and white human hair) using Raman spectroscopy. *Biopolymers* **81**, 506-514 (2006). https://doi.org:https://doi.org/10.1002/bip.20453
43. Bazylewski, P., Divigalpitiya, R. & Fanchini, G. In situ Raman spectroscopy distinguishes between reversible and irreversible thiol modifications in l-cysteine. *RSC Advances* **7**, 2964-2970 (2017). https://doi.org:10.1039/C6RA25879D
44. Adams, L., Oki, A., Grady, T., McWhinney, H. & Luo, Z. Preparation and characterization of sulfonic acid-functionalized single-walled carbon nanotubes. *Physica E: Low-dimensional Systems and Nanostructures* **41**, 723-728 (2009). https://doi.org:https://doi.org/10.1016/j.physe.2008.11.018
45. Blanco-Brieva, G., Campos-Martin, J. M., Frutos, M. P. d. & Fierro, J. L. G. Preparation, Characterization, and Acidity Evaluation of Perfluorosulfonic Acid-Functionalized Silica Catalysts. *Industrial & Engineering Chemistry Research* **47**, 8005-8010 (2008). https://doi.org:10.1021/ie800221f
46. Ganesan, P., Sivanantham, A. & Shanmugam, S. Inexpensive electrochemical synthesis of nickel iron sulphides on nickel foam: super active and ultra-durable electrocatalysts for alkaline electrolyte membrane water electrolysis. *Journal of Materials Chemistry A* **4**, 16394-16402 (2016). https://doi.org:10.1039/C6TA04499A
47. Nasef, M. M. & Saidi, H. Surface studies of radiation grafted sulfonic acid membranes: XPS and SEM analysis. *Applied Surface Science* **252**, 3073-3084 (2006). https://doi.org:https://doi.org/10.1016/j.apsusc.2005.05.013
48. Wu, Q., Jungstedt, E., Šoltésová, M., Mushi, N. E. & Berglund, L. A. High strength nanostructured films based on well-preserved β-chitin nanofibrils. *Nanoscale* **11**, 11001-11011 (2019). https://doi.org:10.1039/C9NR02870F
49. Ki, C. S., Kim, J. W., Oh, H. J., Lee, K. H. & Park, Y. H. The effect of residual silk sericin on the structure and mechanical property of regenerated silk filament. *International Journal of Biological*

Macromolecules **41**, 346-353 (2007). https://doi.org:https://doi.org/10.1016/j.ijbiomac.2007.05.005

50. Huang, Q. M. *et al.* Methanol permeability and proton conductivity of Nafion membranes modified electrochemically with polyaniline. *Journal of Power Sources* **184**, 338-343 (2008). https://doi.org:https://doi.org/10.1016/j.jpowsour.2008.06.013
51. Dandurand, J. *et al.* Conformational and thermal characterization of a synthetic peptidic fragment inspired from human tropoelastin: Signature of the amyloid fibers. *Pathologie Biologie* **62**, 100-107 (2014). https://doi.org:https://doi.org/10.1016/j.patbio.2014.02.001
52. Vilekar, S. A. & Datta, R. The effect of hydrogen crossover on open-circuit voltage in polymer electrolyte membrane fuel cells. *Journal of Power Sources* **195**, 2241-2247 (2010). https://doi.org:https://doi.org/10.1016/j.jpowsour.2009.10.023
53. Ramaswamy, N., Hakim, N. & Mukerjee, S. Degradation mechanism study of perfluorinated proton exchange membrane under fuel cell operating conditions. *Electrochimica Acta* **53**, 3279-3295 (2008). https://doi.org:https://doi.org/10.1016/j.electacta.2007.11.010
54. Gubler, L., Dockheer, S. M. & Koppenol, W. H. Radical (HO•, H• and HOO•) Formation and Ionomer Degradation in Polymer Electrolyte Fuel Cells. *Journal of The Electrochemical Society* **158**, B755 (2011). https://doi.org:10.1149/1.3581040
55. Francia, C., Ijeri, V. S., Specchia, S. & Spinelli, P. Estimation of hydrogen crossover through Nafion® membranes in PEMFCs. *Journal of Power Sources* **196**, 1833-1839 (2011). https://doi.org:https://doi.org/10.1016/j.jpowsour.2010.09.058
56. Li, S., Wei, X., Dai, H., Yuan, H. & Ming, P. Voltammetric and galvanostatic methods for measuring hydrogen crossover in fuel cell. *iScience* **25**, 103576 (2022). https://doi.org:10.1016/j.isci.2021.103576
57. Schoemaker, M., Misz, U., Beckhaus, P. & Heinzel, A. Evaluation of Hydrogen Crossover through Fuel Cell Membranes. *Fuel Cells* **14**, 412-415 (2014). https://doi.org:https://doi.org/10.1002/fuce.201300215
58. Kim, Y., Ketpang, K., Jaritphun, S., Park, J. S. & Shanmugam, S. A polyoxometalate coupled graphene oxide–Nafion composite membrane for fuel cells operating at low relative humidity. *Journal of Materials Chemistry A* **3**, 8148-8155 (2015). https://doi.org:10.1039/C5TA00182J

Figures

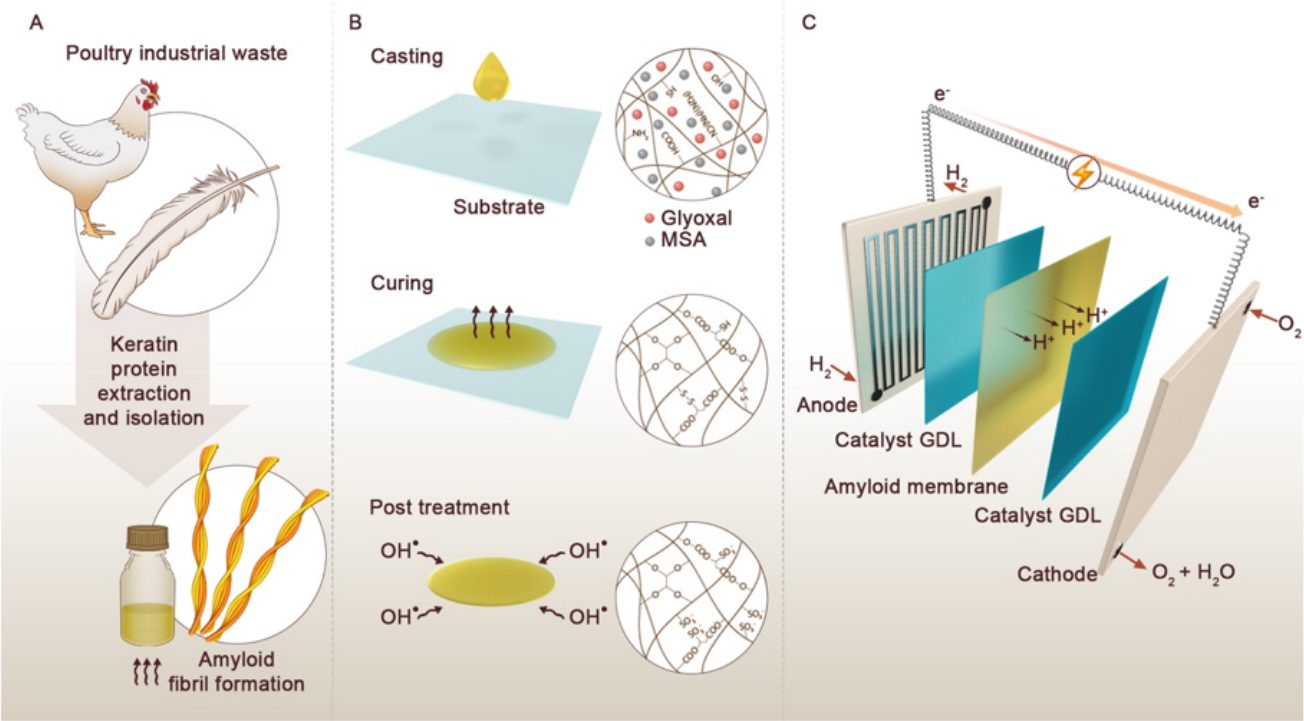

Figure 1

General schematic of the valorization of chicken feather keratin for fuel cell applications. **a**, Extraction, isolation, and amyloid fibril formation of feather keratin. **b**, Membrane fabrication through solvent casting, thermal curing, and post treatment. **c**, Application of keratin membrane into a fuel cell assembly.

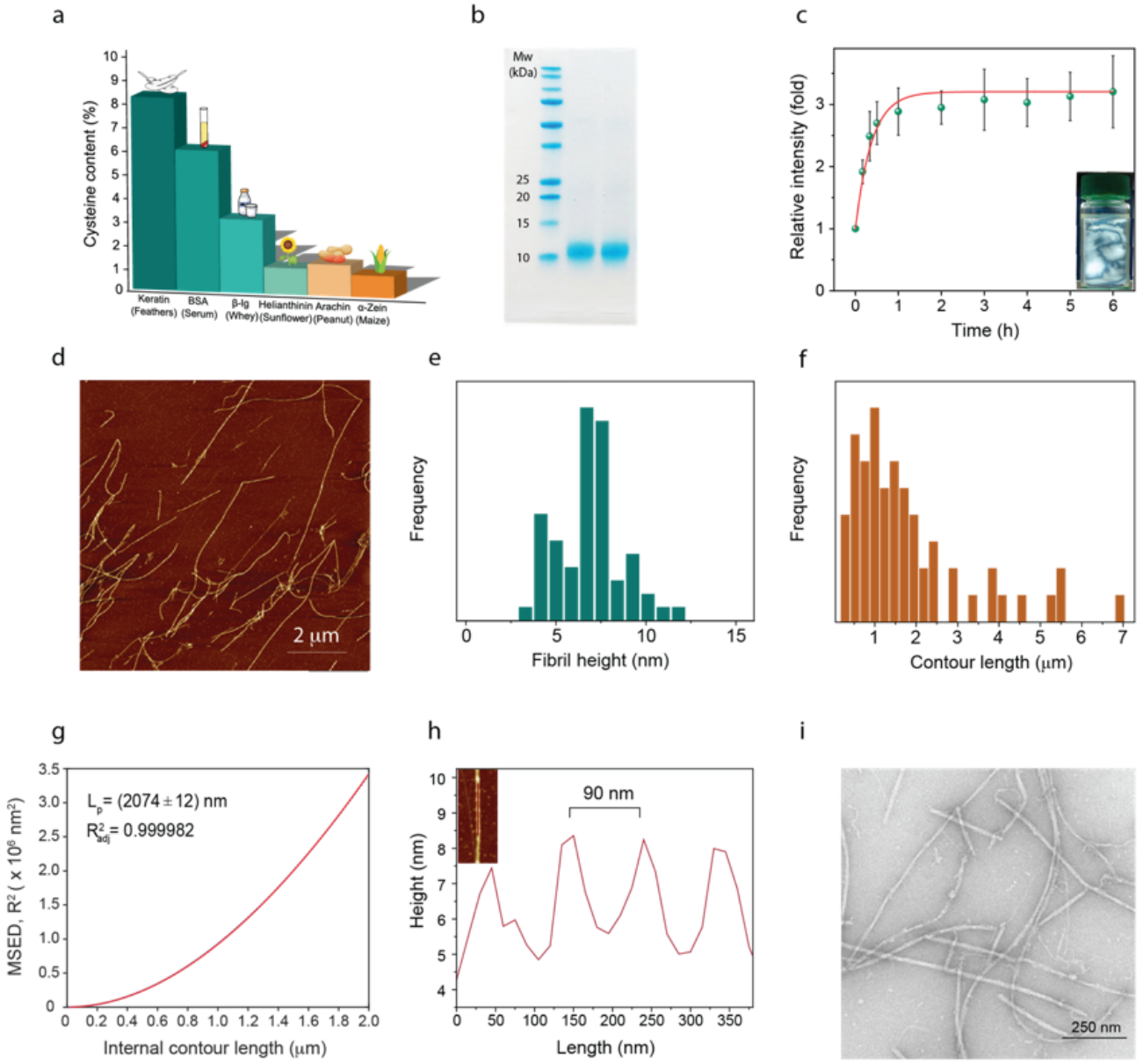

Figure 2

a, Comparison of Cys content in several major proteins from industrial food waste. **b**, SDS-PAGE of isolated feather keratin with and without reducing agent, respectively. **c**, Fibrillization behavior of feather keratin amyloid fibrils with time, as assessed with thiazole orange. Inset: amyloid fibril solution under cross-polarized light. **d**, AFM image of feather keratin amyloid fibrils. **e-ih**, AFM statistical analysis of feather keratin amyloid fibrils showing average fibril height (e); contour length (f); persistence length L_p (g) obtained through the 2D mean square end-to-end displacement (MSED) method; and fibril pitch (h). **i**, TEM images of feather keratin amyloid fibrils.

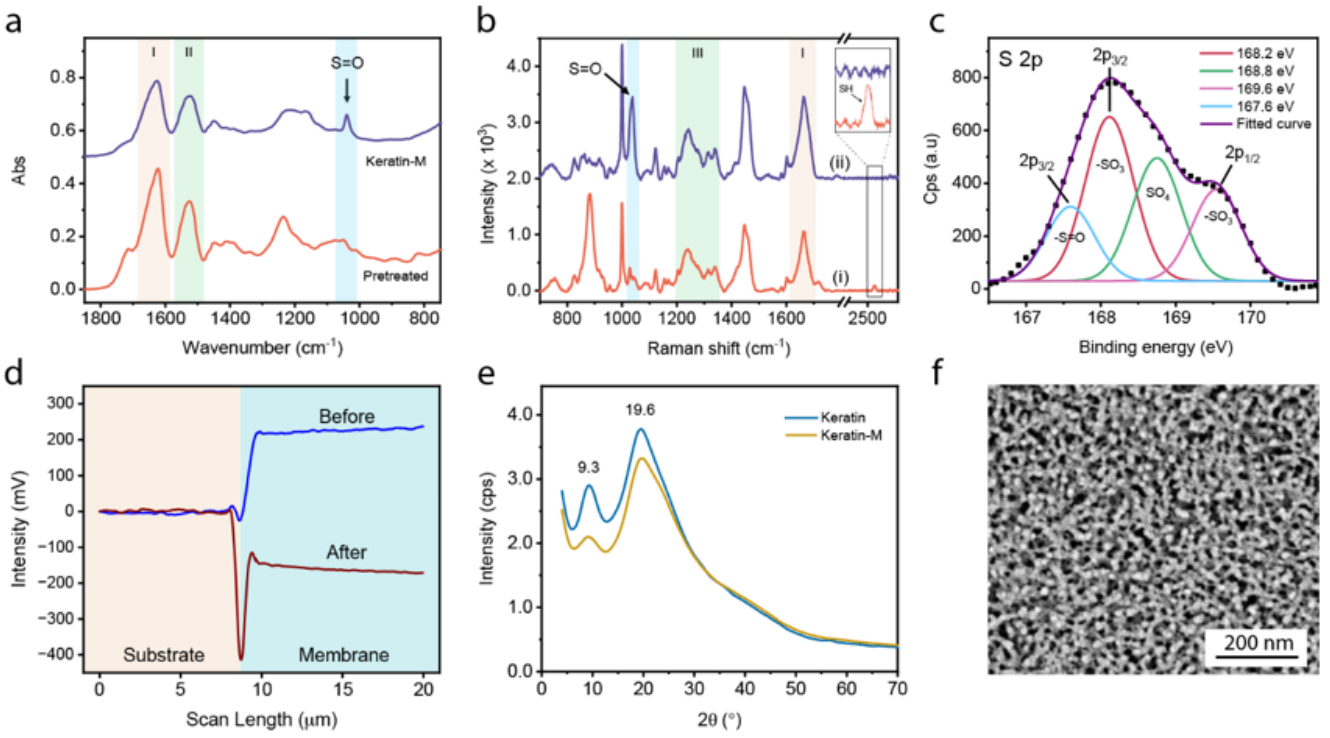

Figure 3

a, FTIR spectra of keratin membranes. **b**, Raman spectra of keratin membranes. **c**, XPS spectrum of the keratin-M membrane. **d**, Surface potential of the keratin-M membrane before and after treatment using KPFM. **e**, XRD patterns of keratin membranes. **f**, SEM image of the keratin-M membrane.

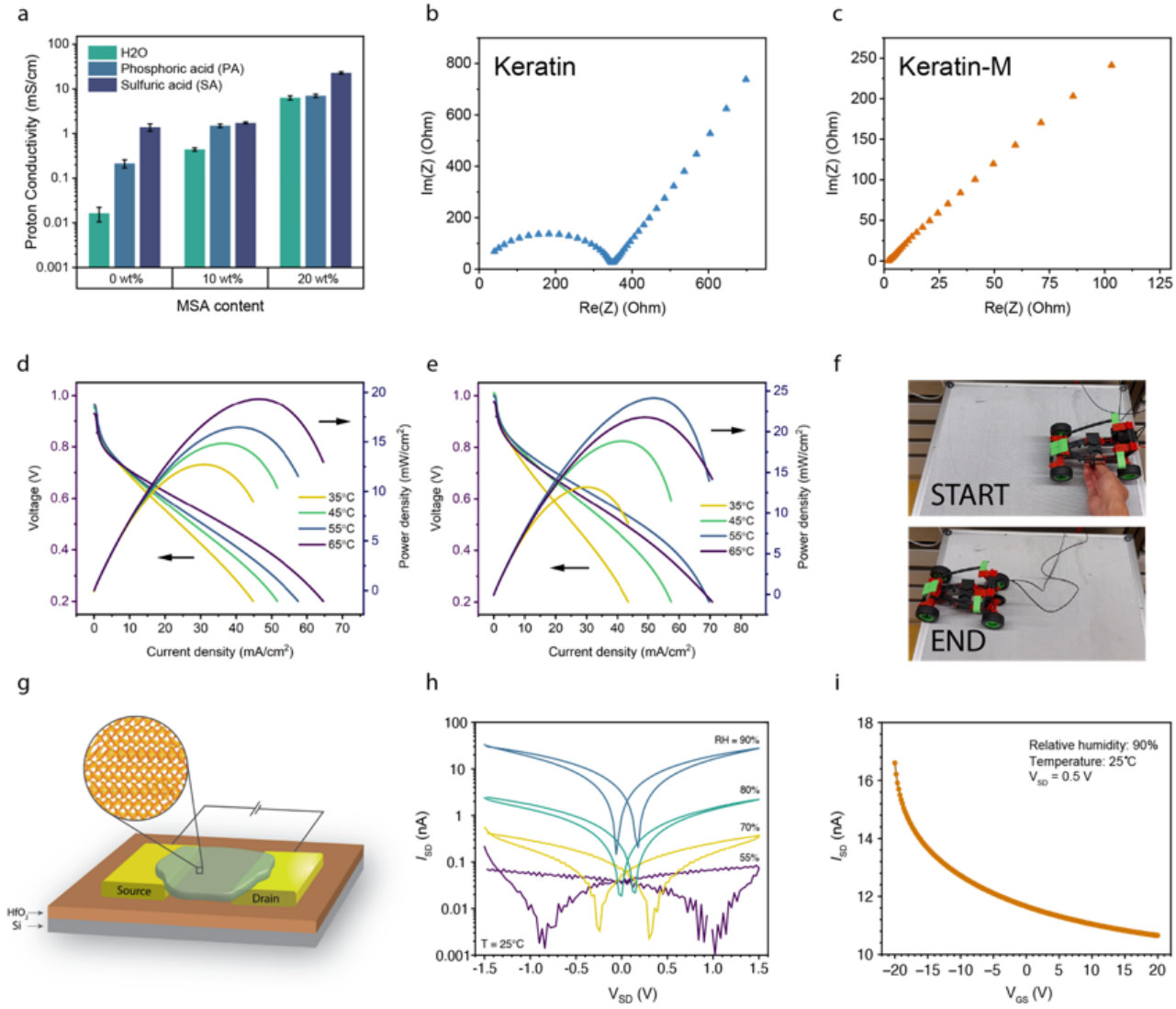

Figure 4

a, Proton conductivity of keratin membranes with increasing MSA content. Nyquist plot of **b**, neat keratin membrane and **c,** keratin-M membrane. In-situ performance of keratin-M membrane at different temperatures using hydrogen at the anode and **d**, Air and **e**, O_2 at the cathode. **f**, Keratin-M membranes assembled into a commercial fuel cell to power a commercial fuel cell toy car. **g**, Schematic illustration of protonic field-effect transistor using keratin-M membrane. **h**, I-V plot of keratin-M on PdH_x electrodes with increasing relative humidity (I_{SD} in log scale). **i,** Transfer characteristic of keratin-M bioprotonic FET device at 90% RH and V_{SD} = 0.5 V on PdH_x electrodes.

Supplementary Files

This is a list of supplementary files associated with this preprint. Click to download.

- SupplementaryMovie1.mp4

- SupplementaryMovie2.mp4
- SupplementaryMovie3.mp4
- SupplementaryMovie4.mp4
- SoonetalSIfinal.docx